# First-Order Transverse Phonon Deformation Potentials of Tetragonal Perovskites

**Marco Deluca and Giuseppe Pezzotti***

*Ceramic Physics Laboratory, Kyoto Institute of Technology, Matsugasaki, Sakyo-ku, 606-8585 Kyoto, Japan*

*Received: June 16, 2008; Revised Manuscript Received: August 19, 2008*

A theoretical formalism is put forward with the aim of describing the softening of first-order transverse optical phonons in a strained tetragonal perovskitic lattice. On the basis of the dynamical equation for nondegenerate polar modes, the influence of oblique phonons could be first described by assuming a prevalence of short-range interatomic forces; then, the softening effect arising from external stress could be explicitly expressed as a function of orientation of the crystallographic texture. As a further step in the adopted formalism, the microstructure of a perovskitic polycrystal has been ideally modeled as an ensemble of mesocrystals, whose individual crystallographic directions corresponded to an average orientation over the unit volume of the probe. An experimental confirmation of the theoretical formalism is concurrently carried out, and phonon deformation potentials (PDP) have been directly measured for the first-order transverse phonon of a tetragonal $PbZrTiO_3$ perovskite lattice.

## I. Introduction

Crystals belonging to the perovskitic family, such as $BaTiO_3$ (BT) and $PbZrTiO_3$ (PZT), have attracted constant interest in the field of ceramic physics due to their ferroelectric behavior and to the peculiarity of their structural phase transitions, which make this class of materials highly suitable for a number of functional applications. The development of ferroelectric domains upon cooling from the Curie temperature and their systematic switching in response to a stress or to an electric field represent the main physical phenomenon behind the dielectric and piezoelectric behavior of the perovskites. A number of researchers have long studied the structural and optical properties of perovskitic structures; in particular, Raman spectroscopy has been regarded as a useful technique for the direct investigation of their lattice properties. On the one hand, basic approaches have been followed to determine the overall lattice dynamics and the nature of polar and oblique phonons by combining polarized micro-Raman measurements and ab initio methods.[1−6] On the other hand, efforts have been also made in clarifying and interpreting how the vibrational properties of perovskite lattices may impact on applicative purposes.[7−12] However, apart from earlier works aimed at retrieving Grüneisen mode parameters under hydrostatic pressure,[13,14] there is yet a lack in fundamental work on the analysis of the effect of external stress fields on first-order optical phonons in perovskites, especially with regard to their oblique phonon characteristics.

In their pioneering work, Maradudin et al.[15] have shown how strain-related morphic effects can be explicitly expressed in terms of microscopic parameters of the crystal (i.e., including force constants and dipole-moment coefficients). In that study, a theoretical characterization of morphic effects enabled those researchers to locate four independent deformation potential parameters and the morphic effect itself was proposed as a means for determining intrinsic physical properties and crystal parameters. However, a remark was also given that such a theoretical assessment could be severely complicated by the large number of atomic-force constants that determine the deformation potentials. In previous works,[10−12] in an effort to overcome the problems encountered in previous researches, we have proposed an experimental method for analyzing domain orientation on a microscopic scale in domain-textured perovskites. This method is based on the quantitative analysis of polarized Raman emission. In those works, emphasis was also placed on examining stress effects on the vibrational characteristics of PZT and BT, although this latter issue could be attempted only from a purely phenomenological point of view.[11] In this work, we build upon previous theories and experimental findings in the attempt to put forward a more general theoretical formalism capable of comprehensively describing the softening of first-order transverse optical phonons generated in a perovskite crystal, thus opening the possibility to directly obtain deformation potential constants from Raman experiments.

This article is organized as follows: (i) a theoretical frame is first drawn in order to comprehensively describe both angular dependence of phonon modes and stress effects in textured polycrystalline perovskites; (ii) the changes in the localized-mode frequencies of separated oblique phonons are then explicitly derived for textured perovskite polycrystals by treating the probe volume as an individual crystal of a mesoscopic dimension; (iii) an experimental verification of the above items (i) and (ii), is concurrently carried out with determining phonon deformation potentials (PDP) through polarized Raman experiments in a polycrystalline PZT, selected as a paradigm perovskitic structure.

## II. Theoretical Framework

**II.A. Raman Effect in Tetragonal Perovskites.** A theoretical treatment is explicitly given here for the tetragonal $C_{4v}$ phase. In such structure, 12 optical modes in the high-temperature cubic phase transform into the $3T_{1u} + T_{2u}$ irreducible representation according to the $O_h$ point group, which consists of a triply degenerate $T_{2u}$ silent (i.e., neither Raman nor infrared active) mode and 3 triply degenerate infrared active $T_{1u}$ modes. In the ferroelectric tetragonal phase, each cubic $T_{1u}$ mode transforms

* To whom correspondence should be addressed. E-mail: pezzotti@kit.ac.jp. Tel. and Fax: +81757247568.

10.1021/jp805278u CCC: $40.75 
Published on Web 10/09/2008

into the $A_1$+E irreducible representation of $C_{4v}$, whereas the silent mode has been reported to undergo a degeneracy-removed state (although this circumstance has not yet been experimentally confirmed[2]). Further splitting of modes can be associated with infrared activity and gives rise to transverse and longitudinal components whose frequencies are generally dependent on propagation directions in the perovskitic crystal lattice. The $A_1$+E modes comprise one transverse E(TO) mode of constant frequency and two mixed modes of combined $A_1$+E symmetry with variable frequency (oblique phonons). For propagation parallel or perpendicular to the *c* axis, the mixed modes become pure E(TO) and $A_1$(LO) or $A_1$(TO) and E(LO) modes, respectively. As far as the $B_1$+E modes are concerned, a transverse E(TO) mode and a mixed $B_1$ mode, each of constant frequency, and a mixed E mode with variable frequency are obtained.

The relative intensity of Raman bands strongly depends on crystal orientation and on the polarization geometry of the adopted optical probe configuration, and can be expressed as:[16]

$$I \propto |\mathbf{e}_i \mathscr{R} \mathbf{e}_s|^2 \tag{1}$$

where $I$ is the reflected Raman intensity, $\mathbf{e}_i$ and $\mathbf{e}_s$ are the unit polarization vectors of the electric field of incident and scattered laser beam, respectively, and $\mathscr{R}$ represents the Raman scattering tensor of the particular band under consideration. Let us consider a reference system in which laser propagation occurs along the *x* axis and is polarized along the *y* axis, whereas the scattered light travels along the *x* direction (true backscattering configuration) and is polarized along either *y* or *z* axis: parallel $x(yy)\bar{x}$ or cross $x(yz)\bar{x}$ configurations, respectively (cf. Porto notation). The second-rank Raman tensor for the $A_g$ and $E_g$ vibrational modes of tetragonal $C_{4v}$ crystal takes the forms given in (2) and (3), respectively:

$$_{Ag} = \begin{pmatrix} a & 0 & 0 \\ 0 & a & 0 \\ 0 & 0 & b \end{pmatrix} \tag{2}$$

$$_{E_g} = \begin{pmatrix} 0 & 0 & 0 \\ 0 & 0 & e \\ 0 & e & 0 \end{pmatrix} \tag{3}$$

as expressed in the crystal principal axes directions according to Nye.[17] The components of the above Raman tensors represent the scattering components along various directions of the tetragonal crystal. The scattering intensities as a function of an in-plane rotation angle $\vartheta$ between the crystallographic *c* axis and the incident polarization vector are obtained upon introducing a transformation matrix of direction cosines, expressed in terms of Euler's angles, and upon rearranging eqs 1–3. The Raman intensities for the $A_g$ and $E_g$ bands can be then expressed as[11]

$$I^{||}_{A_g} \propto |a \cos^2 \vartheta + b \sin^2 \vartheta|^2 = C_1 + C_2 \cos 2\vartheta + C_3 \cos 4\vartheta \tag{4}$$

$$I^{\perp}_{A_g} \propto |(b-a) \sin \vartheta \cos \vartheta|^2 = C_4 - C_5 \cos 4\vartheta \tag{5}$$

$$I^{||}_{Eg} \propto |2e \sin \vartheta \cos \vartheta|^2 = C'_1 - C'_2 \cos 4\vartheta, \tag{6}$$

$$I^{\perp}_{E_g} \propto |e(\cos^2 \vartheta - \sin^2 \vartheta)|^2 = C'_3 + C'_4 \cos 4\vartheta \tag{7}$$

where the superscripts || and ⊥ refer to parallel $x(yy)\bar{x}$ and cross $x(yz)\bar{x}$ polarized configurations for the scattered light, respectively. The parameters $C_i$ and $C'_i$ ($i = 1-5$) are functions of the Raman scattering components and of the instrumental configuration of the analytical device used; in addition, they depend on the degree of texture of the polycrystal. Eqs 4−7 can be generally used for describing the angular dependence of optical modes intensity in tetragonal perovskites belonging to the $C_{4v}$ point group.

Inasmuch as we refer to oblique phonon frequencies of a crystal with uniaxial $C_{4v}$ symmetry, the dielectric constant as a function of spectral frequency, $\omega$, and angular orientation $\vartheta$, can be given by[18]

$$\varepsilon(\omega, \vartheta) = \varepsilon_c(\omega) \cos^2 \vartheta + \varepsilon_a(\omega) \sin^2 \vartheta \tag{8}$$

where $\varepsilon_a(\omega)$ and $\varepsilon_c(\omega)$ are the dielectric constants along the *a* and *c* axes (both functions of $\omega$), respectively, and can be expressed according to the Kurosawa's relation:[19]

$$\frac{\varepsilon_a(\omega)}{\varepsilon_a(\infty)} = \frac{\prod_{j=1}^{4} [(\omega^{LO}_{E(j)})^2 - \omega^2]}{\prod_{j=1}^{4} [(\omega^{TO}_{E(j)})^2 - \omega^2]} \tag{9}$$

$$\frac{\varepsilon_c(\omega)}{\varepsilon_c(\infty)} = \frac{\prod_{j=1}^{3} [(\omega^{LO}_{A_1(j)})^2 - \omega^2]}{\prod_{j=1}^{3} [(\omega^{TO}_{A_1(j)})^2 - \omega^2]} \tag{10}$$

where $\omega^{TO}_{E(j)}$, $\omega^{LO}_{E(j)}$, $\omega^{TO}_{A_1}(j)$, and $\omega^{LO}_{A_1}(j)$ are polar mode frequencies of the E($TO_j$), E($LO_j$), $A_1$($TO_j$), and $A_1$($LO_j$) modes, respectively, and $\varepsilon_a(\infty)$, $\varepsilon_c(\infty)$ are the dielectric constants at frequencies much larger as compared to lattice vibrations. Introducing eqs 9 and 10 into eq 8, the Merten's equation is obtained, as follows:[20]

$$\varepsilon_c(\infty) \cos^2 \vartheta \prod_{j=1}^{3} [(\omega^{LO}_{A_1(j)})^2 - \omega^2] \prod_{j=1}^{4} [(\omega^{TO}_{E(j)})^2 - \omega^2] + \varepsilon_a(\infty) \sin^2 \vartheta \prod_{j=1}^{4} [(\omega^{LO}_{E(j)})^2 - \omega^2] \prod_{j=1}^{3} [(\omega^{TO}_{A_1(j)})^2 - \omega^2] = 0 \tag{11}$$

This equation provides the link between band frequencies, $\omega$, of oblique phonon and a given $\vartheta$ direction. Under the assumption that short-range interatomic forces may prevail on electrostatic forces, the above equations may be rewritten in a simplified form, as follows:

$$\omega^2_{LO} = (\omega^{LO}_{A_1(j)})^2 \cos^2 \vartheta + (\omega^{LO}_{E(j)})^2 \sin^2 \vartheta \tag{12}$$

$$\omega^2_{TO} = (\omega^{TO}_{E(j)})^2 \cos^2 \vartheta + (\omega^{TO}_{A_1(j)})^2 \sin^2 \vartheta \tag{13}$$

where $\omega_{LO}$ and $\omega_{TO}$ are the frequency of the oblique phonons relating the polar mode $A_1$($LO_j$) to E($LO_j$) and $A_1$($TO_j$) to E($TO_j$), respectively.

**II.B. Stress Morphic Effect in Tetragonal Perovskites.** In the presence of strain, the dynamical equation, which links each nondegenerate optical phonon of a tetragonal perovskite to terms linear in the strain, has the form[21]

$$K_{ij}\xi_j = \omega^2 \xi_i \tag{14}$$

where $K_{ij}$ are elements of the force constant tensor, $\omega$ is the Raman frequency in presence of strain, and $\xi_i$ are eigenvectors

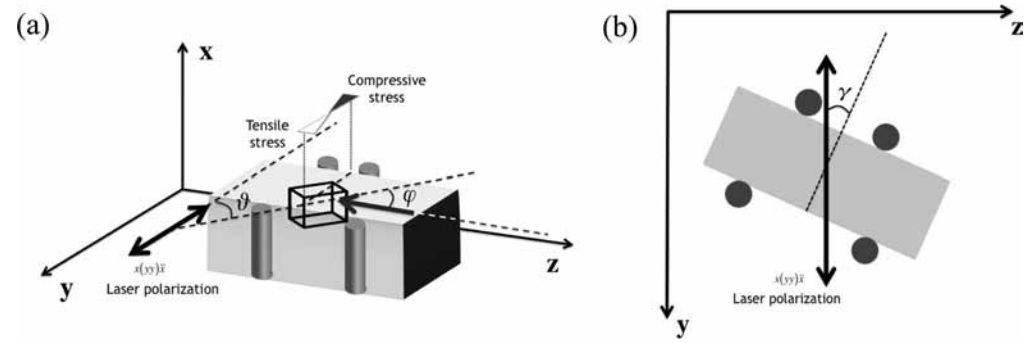


**Figure 1.** (a) Draft of the experimental setup also showing the Cartesian coordinate system of our choice. The position of a mesocrystal is arbitrarily drawn with respect to the stress axis and to the laser polarization direction. (b) Definition of the angle $\gamma$ as the in plane rotation angle of a sample subjected to 4-point bending with respect to a fixed laser polarization direction.

in the crystal reference system. The components $K_{ij}$ can be expanded in the following:

$$K_{ij} = K_{ij}^{(0)} + \sum_{kl} \varepsilon_{kl} K_{ijkl}^{(\varepsilon)} = \omega_0^2 \delta_{ij} + \sum_{kl} \varepsilon_{kl} \frac{\partial K_{ij}}{\partial \varepsilon_{kl}} \qquad (15)$$

where $\varepsilon_{kl}$ are the strain tensor components in the crystal reference system, $\omega_0$ is the phonon frequency in the absence of strain, and $K_{ijkl}^{(\varepsilon)}$ is the tensor of PDP. In a tetragonal $C_{4v}$ crystal, $K_{ijkl}^{(\varepsilon)}$ in principle consists of six independent components.[17] Substituting for eq 15 into eq 14 yields the secular equation for nondegenerate phonon modes in form of a rank-one matrix whose eigenvalue, $\lambda$, represents the Raman frequency shift in the presence of strain:

$$|(K_{11}\varepsilon_{11} + K_{12}\varepsilon_{22} + K_{13}\varepsilon_{33}) - \lambda| = 0 \qquad (16)$$

where $K_{11}$, $K_{12}$, and $K_{13}$ are the nonzero components of the PDP tensor. It can be immediately noted from eq 16 that the Raman shift of nondegenerate optical modes in tetragonal perovskites solely depends on hydrostatic strain components. Small frequency shifts with respect to a nonstrained frequency can be then represented according to the following approximated expression:

$$\lambda = \omega^2 - \omega_0^2 = (\omega - \omega_0)(\omega + \omega_0) \approx 2\omega_0 \Delta\omega \qquad (17)$$

On the other hand, the matrix of elastic compliances governs the relationship between strain and stress in a tetragonal structure, that is, according to the following tensorial equation:

$$\begin{pmatrix} \varepsilon_{11} \\ \varepsilon_{22} \\ \varepsilon_{33} \\ 2\varepsilon_{23} \\ 2\varepsilon_{13} \\ 2\varepsilon_{12} \end{pmatrix} = \begin{pmatrix} S_{11} & S_{12} & S_{13} & 0 & 0 & 0 \\ S_{12} & S_{11} & S_{13} & 0 & 0 & 0 \\ S_{13} & S_{13} & S_{33} & 0 & 0 & 0 \\ 0 & 0 & 0 & S_{44} & 0 & 0 \\ 0 & 0 & 0 & 0 & S_{44} & 0 \\ 0 & 0 & 0 & 0 & 0 & S_{66} \end{pmatrix} \begin{pmatrix} \sigma_{11} \\ \sigma_{22} \\ \sigma_{33} \\ \sigma_{23} \\ \sigma_{13} \\ \sigma_{12} \end{pmatrix} \qquad (18)$$

Values for the elastic compliance parameters of PZT have been partly reported[22] as: $S_{11} = 12.2 \times 10^{-9}$ [GPa]$^{-1}$, $S_{12} = -4.1 \times 10^{-9}$ [GPa]$^{-1}$, $S_{13} = -5.8 \times 10^{-9}$ [GPa]$^{-1}$, $S_{33} = 14.6 \times 10^{-9}$ [GPa]$^{-1}$, and $S_{44} = 32 \times 10^{-9}$ [GPa]$^{-1}$. Please note that these numerical values refer to a random orientation of a PZT polycrystal.

## III. Experimental Methods

Spectroscopic experiments were performed with a microprobe Raman apparatus (T-64000, Horiba/Jobin-Yvon, Kyoto - Japan) equipped with a single monochromator and a liquid nitrogen-cooled Charge Coupled Device (CCD). The 488 nm excitation line of an argon-ion laser (Stabilite 2017; Spectra Physics, Mountain View, CA) was employed and the beam was focused onto the sample with an optical microscope (100X magnification), which allowed us to focus the laser beam waist to about 1 $\mu$m in diameter.

Spectra were collected in a backscattering geometry using sheet polarizers, while a half-wave plate was employed in order to compensate for the polarization dependence of the monochromator. The reference system was chosen with the propagating laser beam coincident with the $x$ axis (i.e., perpendicular to the free surface of the sample), and both incident and scattered light vectors polarized along the $y$ axis in a parallel configuration $x(yy)\bar{x}$, according to Porto notation (cf. draft in part a of Figure 1). Samples were examined in the $yz$ plane, and an angle $\varphi$ was defined as the angle between the main axis of the perovskite mesocrystal and the stress axis. The angle was selected in a way that $\varphi = 0$ corresponds to the $c$ axis of the textured tetragonal structure coincident with the $z$ axis.

Spectral fitting was performed with the help of commercially available software (Labspec 4.02, Horiba/Jobin-Yvon, Kyoto, Japan), according to mixed Gaussian/Lorentzian peak functions after subtracting a linear baseline.

The investigated sample consisted of a mirror-polished poled tetragonal ferroelectric PZT polycrystal ($PbZrTiO_3$)−PNN ($PbNbNiO_3$)−PZN ($PbZnNbO_3$) (simply referred to as PZT−PNN−PZN, henceforth), kindly supplied by Taiyo Yuden Co. Ltd. (Gunma, Japan), shaped as parallelepiped bars with 25 × 3 × 1 mm dimensions and average grain size of about 1 $\mu$m. Poling under a dc field of 2 kV/mm at 150 °C ensured a high degree of polarization/texture in the material. Poled samples were mounted into a four-point flexural jig and loaded close to their tensile strength. The upper and lower spans of the flexural jig were 18 and 6 mm, respectively. A rotation of the sample by an angle, $\gamma$, under polarized light (cf., part b of Figure 1) was performed by means of a special rotating jig, whose eucentricity was achieved by carefully aligning the jig center with the microscope focal axis. The same jig was subsequently used for 4-point bending PS calibrations at various angles. For the PZT−PNN−PZN sample, the in-plane and in-depth laser probe sizes were assessed according to experimental scans across a sharp bimaterial interface and by defocusing experiments, respectively.[23,24] The probe lateral size was defined as twice the distance between the geometrical center of the probe and the point at which 90% of the light was collected, whereas the in-depth probe size was defined as the depth contributing up to 90% to the collected intensity signal. Such sizes were measured as 5.2 and 31 $\mu$m, respectively. In other words, the mesocrystals into which we discretized our textured polycrystal were ap-

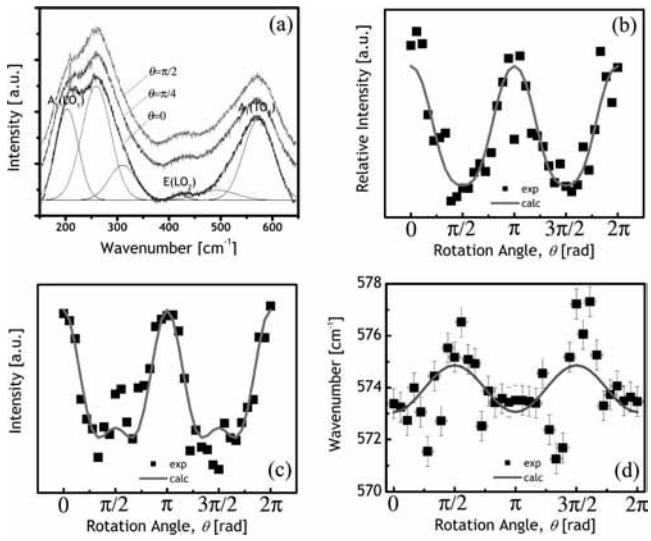


**Figure 2.** (a) Portion of Raman spectra collected on polycrystalline PZT−PNN−PZN at $\vartheta = 0, \pi/4, \pi/2$, with $x(yy)\bar{x}$ polarization. Modes object of our study and overall fitting by Gaussian/Lorentzian modes are indicated. (b) Relative intensity of $A_1(LO_1)$ and $E(LO_2)$ modes. Solid curve represents fitting according to the ratio of eqs 4 and 6. (c) Angular dependence of the intensity and (d) of the wavenumber shift of the $A_1(TO_4)$ optical mode. Solid curves represent fitting to theoretical eqs 4 and 13, respectively.

proximately shaped as cylinders with few micrometers and tens of micrometers of diameter and length, respectively.

## IV. Results and Discussion

**IV.A. Raman Tensor Components of Tetragonal Perovskite Mesocrystal.** The Raman spectrum of PZT−PNN−PZN polycrystal is depicted in part a of Figure 2. The vibrational modes object of this study, are also explicitly indicated, whereas the criterion adopted for fitting is provided for each optical mode. The labeling of the observed modes takes into account the $B_1 + E_g$ feature as suggested by Brya.[6] Three spectra taken at three different orientations of the sample with respect to laser polarization are provided, from which it can be easily noted that differences in relative intensity of modes arise upon changing the angle $\vartheta$.

In Raman experiments, the observed spectrum is representative of the matter comprised within the selected probe, whose volume in turn depends on the material absorption characteristics and may greatly vary not only among types of material but also between the single-crystal and the polycrystalline form of the same material. Accordingly, any local property such as lattice strain, crystal orientation, or chemical gradient can be observed in the Raman spectrum as an average value (i.e., weighted through a probe response function) within the probe, which is generally of Gaussian and Lorentzian nature in the case of in-plane or in-depth probe response, respectively.[23−25] In poled ferroelectrics, each probed location consists of a variety of crystallographic domains oriented at slightly different angles, but all converging toward a preferential axis (i.e., that corresponding to the poling direction). In other words, for each individual portion of probed volume, it is possible to assign an average orientation angle, $\bar{\vartheta}$, comprising the main crystal axis and the polarization direction of the incident laser. This approach is equivalent to consider each probed unit of volume as a single crystal oriented at $\bar{\vartheta}$, and the whole poled polycrystalline body as an ensemble of such crystals, which we will henceforth refer to as mesocrystals to emphasize their mesoscopic nature in a scale lying in between the actual (microscopic) domain size and the (macroscopic) size of the polycrystal (cf. section III). Poled ferroelectric polycrystals exhibit features common to single-crystalline material, for example, anisotropic mechanical properties, optical activity, and scattering behavior. In particular, a geometrical rotation under polarized light performed over textured areas allows one to collect (polarized) scattered light with sinusoidal intensity dependence, whereas random areas give a constant intensity response. The mesocrystal approach can be particularly useful in investigating the angular dependence of optical modes in polycrystalline perovskites (i.e., also given the unavailability of single crystals of large size) because it enables one to assign an individual (average) value of orientation angle to partly textured zones. We shall confirm here the validity of this approach by explicitly reporting the experimentally retrieved intensity and frequency dependence of the $A_1(TO_4)$ mode in PZT−PNN−PZN (shown in parts c and d of Figure 2, respectively), whereas the sinusoidal dependence of the relative intensity of $A_1(LO_1)$ and $E(LO_2)$ bands (shown in part b of Figure 2) has been concurrently used for each experimental point to determine the orientation of the mesocrystal (angle $\bar{\vartheta}$). Solid lines represent least-squares fitting curves according to theoretical equations (eqs 4 and 13 and the ratio of eq 4 to eq 6). Experimental data were acquired while maintaining constant the probe volume, therefore the retrieved angle $\bar{\vartheta}$ represents the mutual orientation between the polarization vector of incident light and the main axis of the mesocrystal. The scattering observed in the data displayed in parts b−d of Figure 2 can be interpreted as an imperfect alignment of the focused beam on the center of the rotating jig, which causes partial averaging over adjacent crystallites. This results in slight modifications of the (average) mesocrystal orientation in each collected spectrum. In particular, part d of Figure 2 presents a high scattering at $\bar{\vartheta} = \pi/4, 5\pi/4$; we interpreted this as because of a surface roughness-driven imperfect perpendicular impingement of the laser beam on the sample surface at those locations. The observed scattering could also be ascribed to an intragranular microtwinned phase, whose presence cannot be in principle ruled out. According to the plots shown in parts b and c of Figure 2, it was possible to characterize the Raman tensor components by retrieving values of −27.48 and −27.20 for $a/e$ and $b/e$, respectively, of the textured PZT−PNN−PZN material.

**IV.B. Phonon Deformation Formalism in Tetragonal Perovskite Mesocrystal.** Because of the presence of oblique phonons, each mode in the Raman spectrum of $C_{4v}$ perovskites requires an examination of both angular-dependent and -independent vibrational modes. Generally, each observed frequency of oblique modes is softened by both the local stress state and the relative orientation of the mesocrystal. The observed oblique mode frequency in each mesocrystal can be defined as follows:

$$\omega_{obs} = \Delta\omega_{stress} + \Delta\omega_{cry} + \omega_0 \tag{19}$$

where $\Delta\omega_{stress}$ is the frequency shift in response to the local stress state, $\Delta\omega_{cry}$ the frequency shift due to the oblique phonon, and is therefore dependent on the angle $\bar{\vartheta}$; $\omega_0$ is the frequency of the optical mode in absence of any external force on the mesocrystal. Substituting for eqs 13 and 17 into 19, it is possible to express the observed frequency shift in terms of both stress morphic effect and local crystal orientation effect:

$$\Delta\omega_{obs} = \omega_{obs} - \omega_0 = \frac{\lambda}{2\omega_0} + \sqrt{\omega^2_{\bar{\vartheta}=0}\cos^2\bar{\vartheta} + \omega^2_{\bar{\vartheta}=\pi/2}\sin^2\bar{\vartheta}} \quad (20)$$

where $\lambda$ is the eigenvalue of the secular equation as defined in (16), $\omega_{\bar{\vartheta}=0}$ and $\omega_{\bar{\vartheta}=\pi/2}$ are the limiting frequencies of the oblique phonon considered. In a mesocrystal, unlike single crystals, the limiting frequencies of the oblique phonon are generally different from pure $A_1$ and $E_g$ modes, as symmetry rules may break down due to grain boundary scattering. For the $A_1(TO_4)$ mode of the PZT−PNN−PZN material investigated in this article, values of 573.06 and 574.86 $cm^{-1}$ were retrieved for $\omega_{\bar{\vartheta}=0}$ and $\omega_{\bar{\vartheta}=\pi/2}$, respectively (i.e., cf. data displayed in part d of Figure 2).

To perform assessments of the stress effect on the Raman spectrum in this class of materials, a known stress state of uniaxial nature was applied. Let us consider a known uniaxial stress field, $\sigma_{33} = \sigma$, directed along the $c$ axis of the tetragonal mesocrystal (i.e., coincident with the $z$ axis in the $yz$ plane; cf. part a of Figure 1). The hydrostatic strains involved with such a stress state can be written as follows, according to eq 18:

$$\varepsilon_{11} = S_{13}\sigma \quad (21)$$

$$\varepsilon_{22} = S_{13}\sigma \quad (22)$$

$$\varepsilon_{33} = S_{33}\sigma \quad (23)$$

which substituted into Eq. (16) give:

$$\lambda = [(K_{11} + K_{12})S_{13} + K_{13}S_{33}]\sigma = \Pi_c\sigma \quad (24)$$

where the phenomenological constant $\Pi_c$ is still a crystal property and has been previously defined as the piezo-spectroscopic (PS) coefficient for the $c$ axis of the tetragonal structure.[10] $\Pi_c$ is a linear combination of the PDP values and is a measurable quantity associated with the polycrystalline material under investigation.

A similar approach considering a known uniaxial stress state along the perpendicular direction gives a PS coefficient for the $a$ axis of the tetragonal mesocrystal structure:

$$\lambda = [K_{11}S_{12} + K_{12}S_{11} + K_{13}S_{13}]\sigma = \Pi_a\sigma \quad (25)$$

In ferroelectric polycrystalline matter, a uniaxial stress state is generally misaligned with respect to both the $c$ and $a$ axes, and the main crystallographic axis is oriented at an angle $\bar{\varphi}$ with respect to the stress axis. Note that $\bar{\varphi}$ is the angle comprising the applied stress direction and the mesocrystal main axis, and it is generally different from the angle, $\bar{\vartheta}$, introduced in section IV.A (cf. part a of Figure 1). The strain calculation then requires the use of a matrix transformation in order to rotate the stress tensor. By assuming a uniaxial stress directed along the $z$ axis, the stress tensor in the mesocrystal can be calculated as follows:

$$\begin{pmatrix} 1 & 0 & 0 \\ 0 & \cos\bar{\varphi} & -\sin\bar{\varphi} \\ 0 & \sin\bar{\varphi} & \cos\bar{\varphi} \end{pmatrix}\begin{pmatrix} 0 & 0 & 0 \\ 0 & 0 & 0 \\ 0 & 0 & \sigma \end{pmatrix}\begin{pmatrix} 1 & 0 & 0 \\ 0 & \cos\bar{\varphi} & \sin\bar{\varphi} \\ 0 & -\sin\bar{\varphi} & \cos\bar{\varphi} \end{pmatrix} = \begin{pmatrix} 0 & 0 & 0 \\ 0 & \sigma\sin^2\bar{\varphi} & -\sigma\sin\bar{\varphi}\cos\bar{\varphi} \\ 0 & -\sigma\sin\bar{\varphi}\cos\bar{\varphi} & \sigma\cos^2\bar{\varphi} \end{pmatrix} \quad (26)$$

This expression in turn leads to the following hydrostatic strain components:

$$\varphi_{11} = (S_{12}\sin^2\bar{\varphi} + S_{13}\cos^2\bar{\varphi})\sigma \quad (27)$$

$$\varepsilon_{22} = (S_{11}\sin^2\bar{\varphi} + S_{13}\cos^2\bar{\varphi})\sigma \quad (28)$$

$$\varphi_{33} = (S_{13}\sin^2\bar{\varphi} + S_{33}\cos^2\bar{\varphi})\sigma \quad (29)$$

Substituting for eqs 27−29 into eq 16, one can obtain a general expression describing the eigenvalue of the secular equation in the case of a uniaxial stress directed along any angle, $\bar{\varphi}$, with respect to the mesocrystal main axis:

$$\lambda = \{[K_{11}S_{12} + K_{12}S_{11} + K_{13}S_{13}]\sin^2\bar{\varphi} + [(K_{11} + K_{12})S_{13} + K_{13}S_{33}]\cos^2\bar{\varphi}\}\sigma = (\Pi_a\sin^2\bar{\varphi} + \Pi_c\cos^2\bar{\varphi})\sigma \quad (30)$$

Similar to the case of eqs 19 and 20, it is therefore possible to write:

$$\Delta\omega_{stress} = \frac{\Pi_a\sin^2\bar{\varphi} + \Pi_c\cos^2\bar{\varphi}}{2\omega_0}\sigma \quad (31)$$

Eq 31 shows that the PS coefficients pertaining the two principal directions of the tetragonal unit cell can be in principle retrieved by applying a known uniaxial stress state to a textured polycrystal oriented along two different directions. It should be noted, however, that this is not easily possible in experimental practice due to the ferroelastic effect. In other words, domain switching will occur in response to the applied strain, partly and locally altering the crystallographic orientation that existed in the sample before the external stress was applied. To overcome this difficulty, we establish here an approach based on eq 31, which provides the link between the local orientation of the mesocrystal and the stress direction. A description is given hereafter for polycrystalline PZT−PNN−PZN, but the procedure is general to ferroelastic materials.

To confirm the theoretical formalism put forward above, a simple experiment can be designed in which a constant uniaxial stress is applied along the $z$ axis in a textured sample loaded in a 4-point bending configuration. Several line scans can be taken at locations across the sample thickness while rotating the sample around the $x$ axis (i.e., according to a stepwise procedure) by an incremental angle, $\gamma$ (cf. draft in part b of Figure 1). Each probed point can be considered to be a mesocrystal according to the aforementioned approach. According to the stress configuration in bending and due to ferroelastic effect, the stress should be approximately directed along the $a$ axis and the $c$ axis of the mesocrystal on the compressive and on the tensile side of the bending bar, respectively. Intermediate orientations are also expected to develop in the textured polycrystal with approaching the neutral axis of the bending bar. In other words, the angle $\bar{\varphi}$ comprising the axis of the mesocrystal and the stress direction is expected to assume different values at each individual location along the profile scan.

In addition, a sample rotation by an angle, $\gamma$, around the $x$ axis is also expected to alter the angle $\bar{\vartheta}$, comprising the main mesocrystal axis and the axis of light polarization; consequently, even if the stress state is kept constant during the experiment, line scans at different rotation angles may lead to different results of wavenumber shift. This difference is depicted in parts a−g of Figures 3 (open circles) in which the $A_1(TO_4)$ optical mode was monitored while rotating the bent bar by increasing $\gamma$ values. Data are heavily scattered due to: (i) a local wavenumber shift of crystallographic origin, $\Delta\omega_{cry}(\bar{\vartheta})$, different at any location (cf. eqs 19 and 20); and, (ii) a variation of the relative orientation of the mesocrystal main axis with respect to the stress

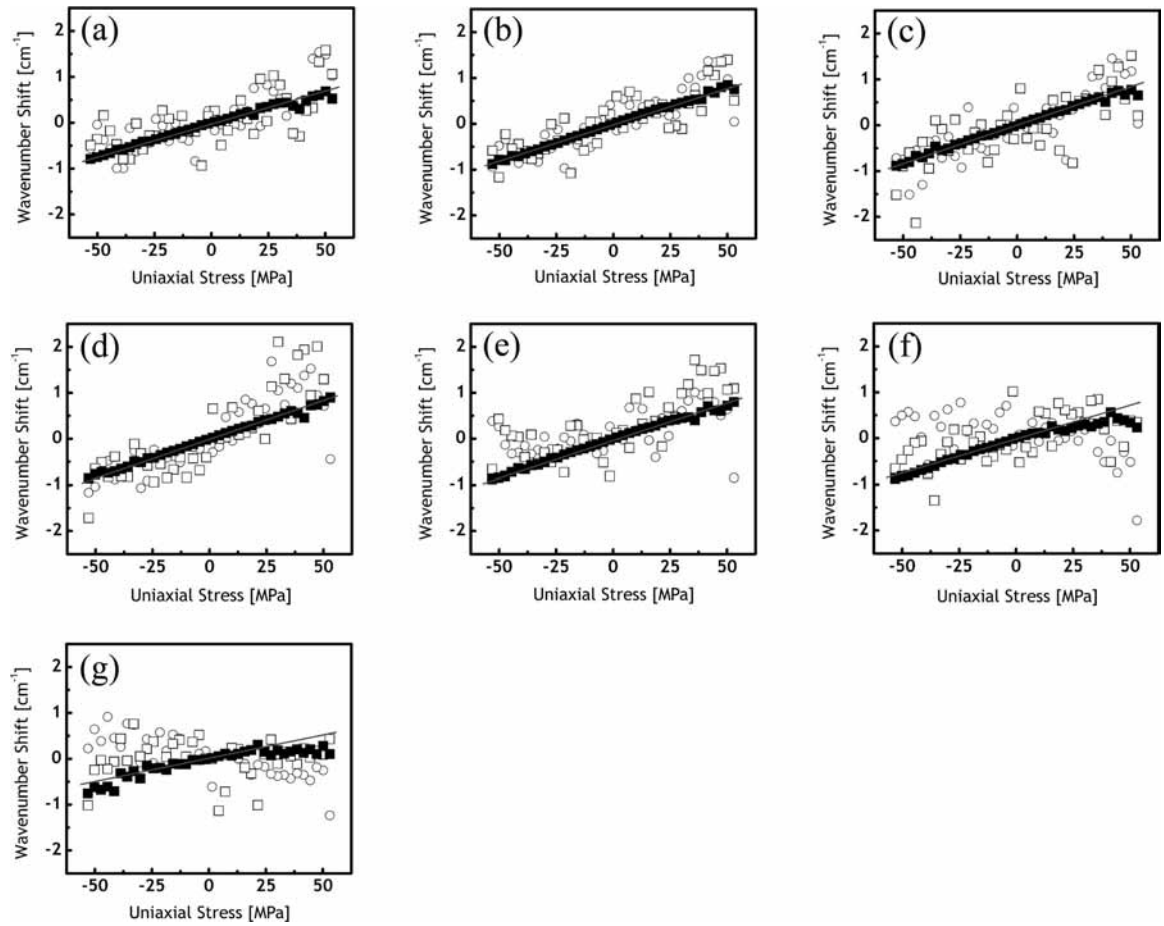


**Figure 3.** Wavenumber change upon uniaxial stress application in a 4-point bending configuration for the $A_1(TO_4)$ mode of ferroelastic PZT−PNN−PZN. Open circles represent the observed wavenumber shift, $\Delta\omega_{obs}$; open squares represent data subtracted of the crystallographic shift according to eq 20 (i.e., $\Delta\omega_{stress}$); closed squares represent further corrected shifts according to eq 31, together with a least-squares fitting procedure to retrieve the PS coefficient values. Dark-gray lines indicate a linear regression of calculated data (closed squares). Data are reported for (a) $\gamma = 0$, (b) $\gamma = \pi/12$, (c) $\gamma = \pi/6$, (d) $\gamma = \pi/4$, (e) $\gamma = \pi/3$, (f) $\gamma = 3\pi/8$, (g) $\gamma = \pi/2$.

direction (angle $\bar{\varphi}$). However, once the direction of the uniaxial stress is known with respect to the fixed reference system, deconvolution of raw data with respect to the above (i) and (ii) phenomena can be performed using the collected spectrum and according to the following steps:

(a) An angle $\bar{\vartheta}$ is assigned to each data point according to the relative intensity of two selected optical modes by means of eqs 4−7.

(b) With the knowledge of the local angle, $\bar{\vartheta}$, it is possible to calculate the angle $\bar{\varphi}$ because the direction of applied stress is kept constant.

(c) The local wavenumber shift arising from the presence of stress can be calculated according to eqs 19 and 20.

(d) Eq 31 is finally used to describe the softening of the considered phonon under the effect of stress.

**IV.C. Phonon deformation potentials of PZT−PNN−PZN.** The formalism put forward in section IV.B is applied in this section to the determination of the PS coefficients for both the *a* and *c* axes, and then of two of the intrinsic PDP values of a PZT−PNN−PZN crystal. In parallel probe configuration, the $A_1(TO_4)$ optical mode at ∼570 cm$^{-1}$ represents a reproducible sensor for stress analysis in PZT crystals, as described in a previous phenomenological study.[11] Using this phonon mode as a sensor, we performed a full rotation in scanning along the thickness of a sample loaded in a 4-point bending configuration (cf. part b of Figure 1). During this procedure, the probed profile was kept constant and a rotation angle, $\gamma$, was applied to the loading apparatus at incremental intervals, as follows: $\gamma = 0$, $\pi/12$, $\pi/6$, $\pi/4$, $\pi/3$, $3\pi/8$, $\pi/2$. Note that prior to the analysis of experimental Raman shifts, data have been subtracted of their respective crystallographic shift components by obtaining the angle $\bar{\vartheta}$ from the relative intensity of the $A_1(LO_1)$ (at ∼210 cm$^{-1}$) and $E(LO_2)$ (at ∼430 cm$^{-1}$) optical modes. Then, the obtained profiles of stress-related wavenumber shifts have been plotted and, considering the linear character expected for a uniaxial stress distribution in a bending bar, a fitting routine has also been run on all the slopes retrieved at different $\gamma$ angles from the experimental plots according to eq 31. According to this latter procedure, the PS coefficients of the $A_1(TO_4)$ phonon could be retrieved as: $\Pi_a/2\omega_0 = 17.12 \pm 0.32$ and $\Pi_c/2\omega_0 = 0.44 \pm 0.06$ cm$^{-1}$/GPa for the *a* and *c* axes of the tetragonal structure of PZT−PNN−PZN, respectively. Line scans of experimental shifts (taken at different $\gamma$ angles) are given in parts a−g of Figure 3. Open circles and squares represent wavenumber shift before and after subtraction of the shift component due to the crystallographic orientation of individual mesocrystals, respectively. Closed squares then represent the shift obtained from the open square data according to eq 31. As can be seen from the high degree of precision in the alignment of the initially scattered data on a linear plot, the established procedure appears to be effective in retrieving the vibrational response of the perovskite crystal to an applied stress. According to the nature of the bending stress applied, we may neglect the strain along the *x* axis (cf., part a of Figure 1) and,

from taking the derivative of eq 30 for two extreme values of $\bar{\varphi}$, obtain a system of two independent linear equations, as follows:

$$\frac{\partial\lambda(\bar{\varphi},z)}{\partial z}_{\bar{\varphi}=0} = (K_{11}+K_{12})S_{13} \quad (32)$$

$$\frac{\partial\lambda(\bar{\varphi},z)}{\partial z}_{\bar{\varphi}=\frac{\pi}{2}} = K_{11}S_{12}+K_{12}S_{11} \quad (33)$$

in which the values of the derivative of the eigenvalue are known (i.e., the measured slopes in parts a and g of Figure 3) and the two deformation potentials $K_{11}$ and $K_{12}$ are the unknown parameters. Regarding the elastic compliance values used in eqs 32 and 33, it should be noted that the literature provides values referring only to a randomly oriented polycrystal, which corresponds to a $\pi/4$ oriented mesocrystal. To retrieve the elastic compliances for the *a* and *c* axes of a single-crystalline structure, therefore, we calculated compliance values using a transformation matrix. The values used in the calculation of PDP are as follows: $S_{11} = 12.9 \times 10^{-9}$ $[\text{GPa}]^{-1}$, $S_{12} = -4.8 \times 10^{-9}$ $[\text{GPa}]^{-1}$, $S_{13} = -5.8 \times 10^{-9}$ $[\text{GPa}]^{-1}$ for the *a* axis and values of $S_{11} = 31.3 \times 10^{-9}$ $[\text{GPa}]^{-1}$, $S_{12} = -23.2 \times 10^{-9}$ $[\text{GPa}]^{-1}$, $S_{13} = -5.8 \times 10^{-9}$ $[\text{GPa}]^{-1}$ for the *c* axis. Upon solving the above system of linear eqs 32 and 33, and using the collected sets of experimental shift, we finally obtain the values: $K_{11}/\omega_0^2 = -17.75$ and $K_{12}/\omega_0^2 = -10.34$ for the tetragonal structure of PZT−PNN−PZN. The choice of the two extreme orientations for the determination of PDP arises from the fact that, in a tetragonal crystal, only mutually perpendicular orientations of ferroelectric domains are possible.

## V. Conclusions

The theory underlying the stress morphic effect of nondegenerate optical phonons in a textured tetragonal perovskite polycrystal has been developed and applied in this article. The consequences involved with considering oblique phonons in a polycrystalline matter have been also taken into account according to what we refer here to as the mesocrystal approach, in which each probe unit was treated as an individual (idealized) single crystal with average crystallographic directions. The theoretical framework has been applied to work out an expression for the PS coefficients pertaining to *a* and *c* axes in tetragonal PZT−PNN−PZN as experimentally accessible parameters, and the PDP values inherent to the perovskitic crystal were finally determined from the dependence of a Raman band position on a known uniaxial stress field. The present approach may hold some generality for the determination of the PDP values in poled and partly textured ferroelastic polycrystals.

## References and Notes

(1) Burns, G.; Scott, B. A. *Phys. Rev. Lett.* **1970**, *25*, 1191.
(2) Burns, G.; Scott, B. A. *Phys. Rev. B* **1973**, *7*, 3088.
(3) Burns, G. *Phys. Rev. B* **1974**, *10*, 1951.
(4) Freire, J. D.; Katiyar, R. S. *Phys. Rev. B* **1988**, *37*, 2074.
(5) Ghosez, P.; Cockayne, E.; Waghmare, U. V.; Rabe, K. M. *Phys. Rev. B* **1999**, *60*, 836.
(6) Brya, W. J. *Phys. Rev. Lett.* **1971**, *26*, 1114.
(7) Li, Z.; Foster, C. M.; Dai, X. H.; Xu, X. Z.; Chan, S. K.; Lam, D. J. *J. Appl. Phys.* **1992**, *71*, 4482.
(8) Nishida, K.; Osada, M.; Wada, S.; Okamoto, S.; Ueno, R.; Funakubo, H.; Katoda, T. *Jpn. J. Appl. Phys* **2005**, *44*, L827.
(9) Cheng, J.; He, L.; Yu, S.; Meng, Z. *Appl. Phys. Lett.* **2006**, *88*, 152906.
(10) Deluca, M.; Sakashita, T.; Pezzotti, G. *Appl. Phys. Lett.* **2007**, *90*, 051919.
(11) Deluca, M.; Sakashita, T.; Zhu, W.; Chazono, H.; Pezzotti, G. *J. Appl. Phys.* **2007**, *101*, 083526.
(12) Deluca, M.; Higashino, M.; Pezzotti, G. *Appl. Phys. Lett.* **2007**, *91*, 091906.
(13) Cerdeira, F.; Holzapfel, W. B.; Bäuerle, D. *Phys. Rev. B* **1975**, *11*, 1188.
(14) Sanjurjo, J. A.; Lopez-Cruz, E.; Burns, G. *Phys. Rev. B* **1983**, *28*, 7260.
(15) Maradudin, A. A.; Ganesan, S.; Burstein, E. *Phys. Rev.* **1967**, *163*, 882.
(16) Loudon, R. *Adv. Phys.* **1964**, *13*, 423.
(17) Nye, J. F. *Physical Properties of Crystals*; Oxford Scientific, Oxford, U.K., 2000.
(18) Jang, M. S.; Takashige, M.; Kojima, S.; Nakamura, T. *J. Phys. Soc. Jpn.* **1983**, *52*, 1025.
(19) Kurosawa, T. *J. Phys. Soc. Jpn.* **1961**, *16*, 1298.
(20) Merten, L. *Phys. Status Solidi* **1968**, *25*, 125.
(21) Anastassakis, E. M. In *Dynamical Properties of Solids*; Horton G. K., Maradudin A., Eds.;North Holland: Amsterdam, The Netherlands, 1980; Vol. 4, p 157.
(22) Moulson, A. J.; Herbert, J. M. *Electroceramics*; Wiley: Southern Gate, U.K., 2003; p 380.
(23) Atkinson, A.; Jain, S. C.; Webbs, S. J. *Semicond. Sci. Technol.* **1999**, *14*, 561.
(24) Atkinson, A.; Jain, S. C. *J. Raman Spectrosc.* **1999**, *30*, 885.
(25) Lipkin, D. M.; Clarke, D. R. *J. Appl. Phys.* **1995**, *77*, 1855.

JP805278U